ELSEVIER

Journal of Fluids and Structures 26 (2010) 747–763

JOURNAL OF FLUIDS AND STRUCTURES

www.elsevier.com/locate/jfs

A fluid–structure interaction model for stability analysis of shells conveying fluid

R.D. Firouz-Abadi, M.A. Noorian, H. Haddadpour*

Department of Aerospace Engineering, Sharif University of Technology, Tehran 11115-8639, Iran

Received 12 March 2009; accepted 14 April 2010
Available online 29 June 2010

Abstract

In this paper, a fluid–structure interaction model for stability analysis of shells conveying fluid is developed. This model is developed for shells of arbitrary geometry and structure and is based on incompressible potential flow. The boundary element method is applied to model the potential flow. The fluid dynamics model is derived by using an inflow/outflow model along with the impermeability condition at the fluid–shell interface. This model is applied to obtain the flow modes and eigenvalues, which are used for the modal representation of the flow field in the shell. Based on the mode shapes and natural frequencies of the shell obtained from an FEM model, the modal analysis technique is used for structural modeling of the shell. Using the linearized Bernoulli equation for unsteady pressure on the fluid–shell interface in combination with the virtual work principle, the generalized structural forces are obtained in terms of the modal coordinates of the fluid flow and the coupled field equations of the fluid–structure are derived. The obtained model is validated by comparison with results in the literature, and very good agreement is demonstrated. Then, some examples are provided to demonstrate the application of the present model to determining the stability conditions of shells with arbitrary geometries.

Keywords: Fluid–structure interaction; Shell; Boundary and finite element methods; Modal analysis technique

1. Introduction

The fluid–structure interaction in shells conveying fluid is considered one of the most important problems in many industrial applications. Some practical examples of this phenomenon occur in the thin-walled cylindrical shells used as thermal shields in the aerospace and power-plant industries, monitoring and control tubes, shells used in heat exchangers and storage tanks, etc. Several studies have been performed on the stability and dynamics of shells conveying fluid, mainly dealing with circular cylindrical shells. A comprehensive review on the dynamics of pipes and shells conveying fluid has been presented by Païdoussis (1998, 2003) in the form of a two-volume book. Furthermore, Païdoussis and Li (1993) produced a review paper with detailed descriptions of almost all of the existing problems in the field of fluid–structure interaction in pipes conveying fluid. Modarres-Sadeghi and Païdoussis (2009) used a weakly nonlinear model to study the post-divergence behavior of extensible fluid-conveying pipes supported at both ends.

*Corresponding author. Tel.: +98 21 66164617; fax: +98 21 66022731.
E-mail addresses: firouzabadi@sharif.edu (R.D. Firouz-Abadi), haddadpour@sharif.edu, haddadpour@gmail.com (H. Haddadpour).

0889-9746/$ - see front matter © 2010 Elsevier Ltd. All rights reserved.
doi:10.1016/j.jfluidstructs.2010.04.003

Through the method of separation of variables, Païdoussis and Denise (1972) presented a traveling-wave-type solution for clamped and cantilevered shells, without satisfying the pertinent boundary conditions. Weaver and Unny (1973) utilized the Fourier transform method to determine the stability conditions of a simply supported cylindrical shell. The main difference between the latter and the former was in the boundary conditions of the outflow. Nguyen et al. (1993) proposed an outflow model to resolve some numerical issues in the previous models when solving the problems of cylindrical fluid-conveying shells and demonstrated that the proposed model converged accurately. Amabili et al. (1999b, 2000a, 2000b, 2002) put forth a comprehensive investigation and review of the linear and nonlinear stability and behavior of circular cylindrical shells conveying fluid. They made use of nonlinear Donnell's shallow shell theory in conjunction with linear potential flow theory to derive their formulation. Amabili and Garziera (2002a) developed the computer program DIVA to analyze the vibrations of cylindrical shells containing or immersed in axial flow. DIVA was capable of considering a wide range of complex effects on the vibrations of circular cylindrical shells, including non-uniform boundary conditions; fluid–structure interaction including both flowing and quiescent fluids as well as internal, external and annular flows; mean radial pressure and initial pre-stress; an elastic bed at partial extension in the circumferential and longitudinal directions; intermediate constraints and added masses. By means of the time-mean Navier–Stokes equations, Amabili and Garziera (2002b) improved DIVA to account for the effects of steady viscous forces on vibrations of shells with internal and annular flow.

Lakis and Laveau (1991) and Selmane and Lakis (1997) used a hybrid finite element method to investigate the nonlinear vibrations of anisotropic cylindrical shells containing fluid. The former was carried out by assuming Sander's linear shell theory and potential flow, while the Bernoulli equation was expanded to the second order. The results showed that in practice, the nonlinearity of the fluid does not significantly affect the stability conditions and can be neglected. The latter research was performed by considering the nonlinear Sanders–Koiter shell alongside the linear potential flow formulation.

Using potential flow theory with Sander's nonlinear theory of thin shells, Zhang et al. (2001) presented a finite element model for investigating fluid–structure vibrations of thin-walled orthotropic cylindrical shells. They also considered the geometric stiffness of the structure due to hydrostatic pressure and initial stress. Hansson and Sandberg (2001) developed a finite element model for fluid–structure interaction in shells by combining an axisymmetric shell element and a one-dimensional fluid element. Kochupillai et al. (2002) employed a semi-analytical finite element formulation in developing model reduction techniques for the analysis of parametric instabilities in flexible pipes conveying fluids under a mean pressure. Kumar and Ganesan (2008) proposed a semi-analytical finite element method for stability analysis of conical fluid-conveying shells and conducted some studies on the critical fluid velocity for conical shells with different cone angles and boundary conditions. Using a coupled boundary-element/finite-element model (BEM-FEM), Shekari et al. (2009) considered the fluid–structure interaction in seismically isolated cylindrical liquid storage tanks. Païdoussis (2005) reviewed some unresolved issues and paradoxes in fluid–structure interaction problems in fluid-conveying pipes and shells. Karagiozis et al. (2005) presented experimental results on the nonlinear dynamics and stability characteristics of thin-walled clamped–clamped circular cylindrical shells. The experiments were carried out for elastomer shells in annular air-flow, elastomer shells with internal air-flow, and aluminum and plastic cylindrical shells with internal water-flow. They discovered a softening nonlinear behavior, with a large hysteresis in the velocity for the onset and cessation of divergence. Karagiozis et al. (2007) investigated the effect of varying the thickness-to-radius and length-to-radius ratios on the stability margin of cylindrical shells conveying fluid. They showed that the system loses stability by a subcritical pitchfork bifurcation, leading to a stable divergence of increasing amplitude with increasing flow speed. Also, Karagiozis et al. (2008) used the Donnell nonlinear shallow shell equations along with linear potential flow theory to investigate the stability and nonlinear behavior of thin, clamped, cylindrical shells. They compared their analytical results with experiments and achieved good qualitative and reasonable quantitative agreement.

Almost all of the existing studies in this area are focused on solving the problem of circular cylindrical shells with the aid of analytical methods. Some researchers have also employed the finite element method to develop fluid–structure interaction models for stability analysis of cylindrical and conical shells conveying fluid. This paper aims to develop a fluid–structure interaction model for shells with arbitrary geometry and structure. The boundary element method is utilized with the potential flow model for fluid dynamics modeling, and the structural model is obtained via the modal analysis technique combined with the finite element model of an arbitrary structure.

2. Structural dynamics

Shell structures are considered important components in many engineering applications, and a number of studies have been performed on the structural dynamics of these shells. Several theories, in both the linear and non-linear domains, for structural dynamics modeling of shells have been presented, considering the effect of thickness, material properties, etc. Despite all of their advantages, the analytical solutions of the problem of shell vibration are limited to simple geometries and cannot be applied to any arbitrary problem. However, numerical techniques, such as the finite

element method (FEM), have been used without such limitations. In general, the governing equation of structural motion in the FEM can be expressed as

$$\mathbf{M}_S\ddot{\mathbf{d}} + \mathbf{C}_S\dot{\mathbf{d}} + \mathbf{K}_S\mathbf{d} = \mathbf{f}, \tag{1}$$

where $\mathbf{M}_S$, $\mathbf{C}_S$ and $\mathbf{K}_S$ are the structural mass, damping and stiffness matrices, respectively. Furthermore, vector $\mathbf{d}$ stands for the nodal displacements and rotations and $\mathbf{f}$ represents the nodal forces and moments.

The FEM can be used with the modal analysis technique to obtain a reduced-order model of the structural dynamics of the shell. The modal expansion of the elastic displacements vector $\mathbf{e}$, and rotations $\boldsymbol{\theta}$ of the shell at each point can be written as

$$\mathbf{e} = \sum_{n=1}^{N_S} \bar{\mathbf{e}}_n \xi_n(t), \quad \boldsymbol{\theta} = \sum_{n=1}^{N_S} \bar{\boldsymbol{\theta}}_n \xi_n(t), \tag{2, 3}$$

where N_S is the number of structural modes and $\bar{\mathbf{e}}_n$ and $\bar{\boldsymbol{\theta}}_n$ are the natural mode shapes of the elastic displacements and rotations, respectively. The mode shapes of the natural vibrations can be calculated simply by using the finite element model along with the standard eigen-analysis methods. The governing equation of the generalized modal coordinates $\boldsymbol{\xi}$ is obtained using the Lagrange equations and Galerkin's method as follows:

$$\ddot{\boldsymbol{\xi}} + \boldsymbol{\Gamma}\dot{\boldsymbol{\xi}} + \boldsymbol{\Omega}\boldsymbol{\xi} = \mathbf{s}, \tag{4}$$

in which $\boldsymbol{\Gamma}$ and $\boldsymbol{\Omega}$ are the diagonal modal damping and stiffness matrices, defined as $\boldsymbol{\Gamma}_{n,n} = 2\zeta_n\omega_n$ and $\boldsymbol{\Omega}_{n,n} = \omega_n^2$, where ζ_n and ω_n are the damping ratio and natural frequency of the nth mode, respectively. Furthermore, $\mathbf{s}$ denotes the vector of generalized structural forces. In general, the natural modes with lower natural frequencies are the major contributors to the structural motion; hence, a system of equations (4) can precisely predict the dynamic behavior of the structure with a small number of the lower frequency modes, truncating the modes at higher frequencies.

3. Fluid dynamics

3.1. Governing equations

Consider a flexible shell with arbitrary geometry and supports, conveying fluid as shown in Fig. 1(a). Assuming incompressible flow in the shell, the Navier–Stokes equations governing the flow field are expressed as

$$\nabla \cdot \mathbf{v} = 0, \tag{5}$$

$$\dot{\mathbf{v}} + (\mathbf{v} \cdot \nabla)\mathbf{v} = -\frac{1}{\rho}\nabla p + \nu\nabla^2\mathbf{v}, \tag{6}$$

where $\mathbf{v}$ is the flow velocity, ρ is the fluid density, ν is the kinematic viscosity and p is the hydrodynamic pressure. If the viscous terms in Eq. (6) are neglected, the flow field can be described using a velocity potential ϕ, from which the velocity can be written as

$$\mathbf{v} = \nabla\phi. \tag{7}$$

Assuming small elastic vibrations of the shell, the potential ϕ can be decomposed into two components: the zeroth-order steady potential $\phi^{(0)}$ due to the mean flow and the first-order unsteady component $\phi^{(1)}$ associated with the shell motion, i.e.,

$$\phi = \phi^{(0)} + \varepsilon\phi^{(1)}, \tag{8}$$

where ε is a small parameter that is merely used to signify the order of magnitude. The zeroth- and first-order potentials satisfy the Laplace equation, i.e.,

$$\nabla^2\phi^{(0)} = 0, \quad \nabla^2\phi^{(1)} = 0. \tag{9, 10}$$

3.2. The wall boundary condition

The impermeability of the shell wall yields the following boundary condition at the fluid–shell interface:

$$\nabla\phi \cdot \mathbf{n} = \varepsilon\mathbf{e} \cdot \mathbf{n}, \tag{11}$$

where the shell motion is assumed to be of the first order of magnitude, and $\mathbf{n}$ represents the outward unit normal vector of the shell, which consists of two components

$$\mathbf{n} = \mathbf{n}^{(0)} + \varepsilon\mathbf{n}^{(1)}, \tag{12}$$

where $\mathbf{n}^{(0)}$ is the normal vector of the undeformed shell, and $\mathbf{n}^{(1)}$ is the small variation of $\mathbf{n}^{(0)}$ due to the deformation of the shell. Assuming small elastic rotations of the shell, the vector $\mathbf{n}^{(1)}$ can be obtained as

$$\mathbf{n}^{(1)} = \boldsymbol{\theta} \times \mathbf{n}^{(0)}. \tag{13}$$

Substituting Eqs. (8) and (12) into Eq. (11) and choosing the terms with identical orders of magnitude, the wall boundary conditions for $\phi^{(0)}$ and $\phi^{(1)}$ can be derived as

$$\nabla\phi^{(0)} \cdot \mathbf{n}^{(0)}|_{\text{wall}} = 0, \tag{14}$$

$$\nabla\phi^{(1)} \cdot \mathbf{n}^{(0)}|_{\text{wall}} = (\dot{\mathbf{e}} \cdot \mathbf{n}^{(0)} - \nabla\phi^{(0)} \cdot \mathbf{n}^{(1)}). \tag{15}$$

3.3. The inflow/outflow boundary conditions

The actual behavior of the fluid at the inlet and outlet of the shell, and its contribution to the physics of the problem are unresolved issues in the field of fluid–structure interaction in shells conveying flow (Païdoussis, 2005). There are some solutions, which are based either on the Fourier transform generalized-force method with the assumption of zero flow perturbations beyond the shell domain (Weaver and Unny, 1973) or the traveling-wave form of the solution, in which the waves continue indefinitely both up and downstream (Païdoussis and Denise, 1972).

For an actual fluid, if a perturbation in the steady flow inside the shell is generated, it will be damped quickly in the upstream region, and thus a constant inflow boundary can be considered a short distance L_i from the shell inlet (Figs. 1(a) and (b)). The perturbation propagates downstream, and it can be assumed that at a distance far enough from the shell outlet, the pressure gradient and the viscous forces in the right-hand side of Eq. (6) are balanced. For inviscid flow, this balanced condition is identical with either a fully developed pressure field in the outflow or a pressure gradient equal to zero. In both cases, the outflow boundary condition can be obtained based on the fact that the flow is fully developed at the outflow, and the fluid particles do not accelerate. In other words, an outflow boundary can be assumed at a distance L_o far enough from the shell outlet that the left-hand side of Eq. (6) is zero (Figs. 1(a) and (b)).

The constant inflow boundary condition is expressed as

$$\nabla\phi \cdot \mathbf{n} = v_i, \tag{16}$$

where v_i is the inflow velocity. The outflow boundary condition is obtained by setting the right-hand side of Eq. (6) equal to zero, namely,

$$\dot{\mathbf{v}} + (\mathbf{v} \cdot \nabla)\mathbf{v} = 0. \tag{17}$$

Note that the convective acceleration $(\mathbf{v} \cdot \nabla)\mathbf{v}$ may also be written in the following form:

$$(\mathbf{v} \cdot \nabla)\mathbf{v} = \tfrac{1}{2}\nabla|\mathbf{v}|^2 - \mathbf{v} \times (\nabla \times \mathbf{v}). \tag{18}$$

For potential flow, the curl of the velocity vanishes, and thus substituting Eq. (7) into (17) yields

$$\nabla(\dot{\phi} + \tfrac{1}{2}|\nabla\phi|^2) = 0. \tag{19}$$

Substituting Eq. (8) into Eq. (16) yields the following inflow boundary conditions:

$$\nabla\phi^{(0)} \cdot \mathbf{n}^{(0)}|_{\text{inflow}} = v_i, \quad \nabla\phi^{(1)} \cdot \mathbf{n}^{(0)}|_{\text{inflow}} = 0. \tag{20, 21}$$

According to the principle of mass conservation, the outflow boundary condition for $\phi^{(0)}$ is

$$\nabla\phi^{(0)} \cdot \mathbf{n}^{(0)}|_{\text{outflow}} = kv_i, \tag{22}$$

where k is the ratio of the outflow area to the inflow area. Introducing Eq. (8) into (19) yields

$$\begin{aligned}(\dot{\phi}^{(0)} + \varepsilon\dot{\phi}^{(1)}) + \tfrac{1}{2}(\nabla\dot{\phi}^{(0)} + \varepsilon\nabla\dot{\phi}^{(1)}) \cdot (\nabla\phi^{(0)} + \varepsilon\nabla\phi^{(1)}) = (\dot{\phi}^{(0)} + \tfrac{1}{2}|\nabla\phi^{(0)}|^2) + (\dot{\phi}^{(1)} + \nabla\phi^{(0)} \cdot \nabla\phi^{(1)})\varepsilon \\ + \text{h.o.t.} = \text{const.}\end{aligned} \tag{23}$$

Balancing the terms at equal orders of ε in Eq. (23) and using Eq. (22) results in the following outflow boundary condition for $\phi^{(1)}$:

$$(\dot{\phi}^{(1)} + kv_i\nabla\phi^{(1)} \cdot \mathbf{n}^{(0)})|_{\text{outflow}} = 0, \tag{24}$$

which implies that the first-order potential wave propagates across the outflow boundary with a velocity of kv_i.

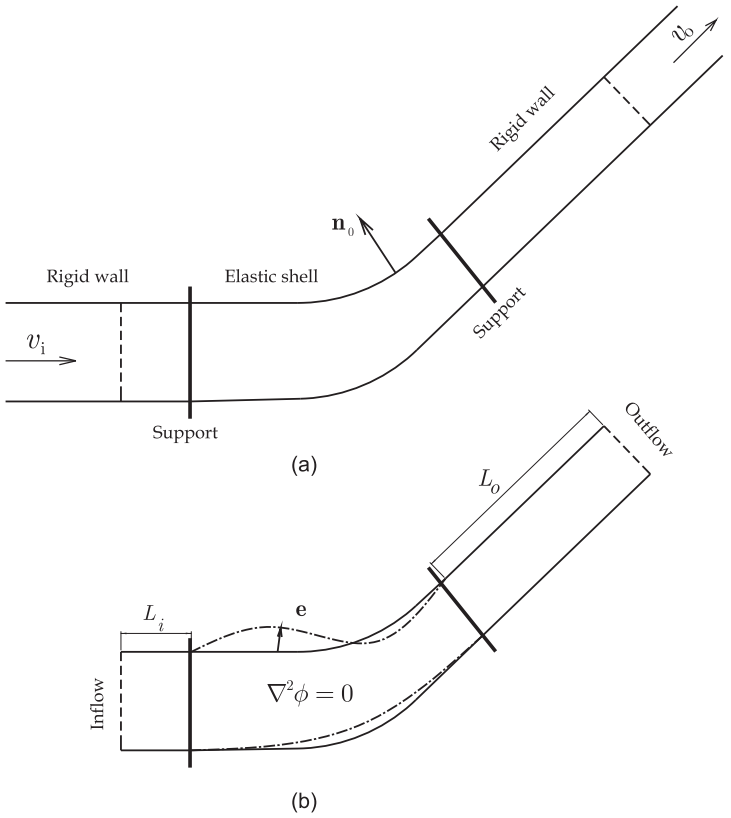

Fig. 1. Schematic figure of flow field and boundaries.

The walls across the inflow boundary near the shell inlet and those across the shell outlet near the outflow boundary are assumed to be rigid walls, namely

$$\nabla\phi^{(0)} \cdot \mathbf{n}^{(0)}|_{\text{r.wall}} = \nabla\phi^{(1)} \cdot \mathbf{n}^{(0)}|_{\text{r.wall}} = 0. \tag{25}$$

3.4. Boundary element modeling

Among the available numerical methods, the boundary element method (BEM) has turned out to be quite popular and has found thriving applications in potential flow problems. Meshing and discretizing the boundaries instead of discretizing the entire fluid domain, and thus cutting down on the necessary memory and computation time, is one of the primary reasons that the BEM is preferred over other methods. For fluid and solid interaction (FSI) problems, one only needs to calculate the fluid data on the fluid–structure interface; hence, another major advantage of using the BEM in FSI problems is that the governing equations of fluid motion are represented only at the boundaries, which reduces unnecessary calculations, such as the velocity or pressure fields inside the fluid domain, that are inevitable in other numerical techniques like the FEM.

In this section, we present the formulation and preliminaries of the BEM to derive the governing equations of the fluid flow in the shell. The solution of the Laplace equation over an unbounded region for a source point of unit strength is the free-space Green's function of the problem. For a three-dimensional space, it is

$$\phi^* = \frac{1}{4\pi r}, \tag{26}$$

where r is the distance from the source point. Applying Green's second identity to the flow region bounded externally by surface S and excluding the sphere of radius ε about point p (see Fig. 2), one obtains

$$\int_{V-V_\varepsilon} (\phi\nabla^2\phi^* - \phi^*\nabla^2\phi)\,\mathrm{d}V = \int_S (\phi q^* - \phi^* q)\,\mathrm{d}S + \int_{S_\varepsilon} (\phi q^* - \phi^* q)\,\mathrm{d}S = 0, \tag{27}$$

where $q=\partial\phi/\partial\mathbf{n}$ and $q^*=\partial\phi^*/\partial\mathbf{n}$. After some mathematical simplifications assuming that ϕ and q are well-behaved functions, the following integral equation is derived from Eq. (27):

$$c_p\phi_p+\int_S(\phi q^*-\phi^* q)\,\mathrm{d}S=0, \tag{28}$$

$$c_p=\frac{\chi}{4\pi}, \tag{29}$$

where χ represents the internal spatial angle viewed from the source point p. If the source point is located on a smooth and flat boundary, then $\chi=2\pi$, and for points inside the flow domain, $\chi=4\pi$.

Eq. (28) can be solved numerically by discretizing the fluid boundary into small elements and calculating the boundary integrals over them, as follows:

$$c_i\phi_i+\sum_{j=1}^{m}\int_{S_j}(q_i^*\phi_j-\phi_i^* q_j)\,\mathrm{d}S_j=0, \tag{30}$$

where m is the number of all boundary elements. The potential and flux density at any point in each element can be approximated by their nodal values by using appropriate interpolation functions.

$$\phi=\mathbf{N}_j\mathbf{u}_j,\quad q=\mathbf{N}_j\mathbf{q}_j, \tag{31,32}$$

where $\mathbf{N}_j$ is a row matrix containing the element shape functions, and $\mathbf{u}_j$ and $\mathbf{q}_j$ are the vectors of nodal potential and flux through the jth element, respectively. Introducing Eqs. (31) and (32) into Eq. (30) and transforming the global coordinate system into the local coordinate system of the boundary elements (x_1, x_2) yields

$$c_i\phi_i+\sum_{j=1}^{m}(\mathbf{H}_{ij}\mathbf{u}_j-\mathbf{G}_{ij}\mathbf{q}_j)=0, \tag{33}$$

in which

$$\mathbf{H}_{ij}=\int_{-1}^{1}\int_{-1}^{1}q_i^*\mathbf{N}_j|\mathbf{J}_j|\,\mathrm{d}x_1\,\mathrm{d}x_2, \tag{34}$$

$$\mathbf{G}_{ij}=\int_{-1}^{1}\int_{-1}^{1}\phi_i^*\mathbf{N}_j|\mathbf{J}_j|\,\mathrm{d}x_1\,\mathrm{d}x_2, \tag{35}$$

where $|\mathbf{J}_j|$ is the determinant of the Jacobian matrix of the transformation from the global Cartesian system to the local coordinate system of the element. Using the point collocation method, Eq. (33) can be evaluated at all boundary nodes and written in the following matrix form:

$$\mathbf{Au}-\mathbf{Bq}=\mathbf{0}, \tag{36}$$

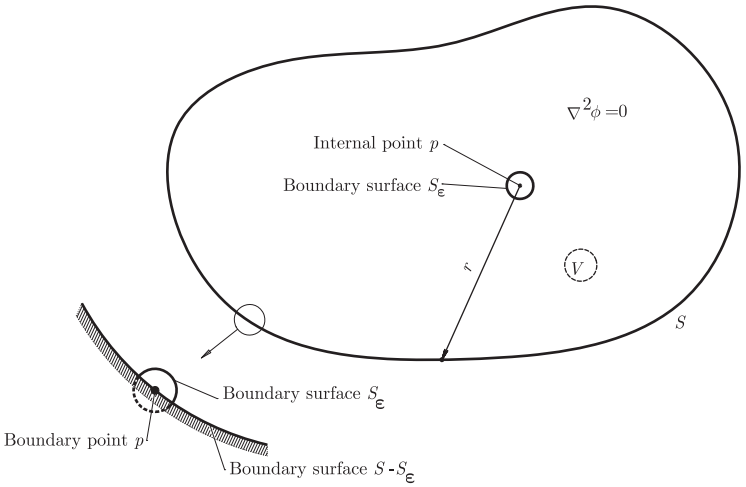

Fig. 2. Schematic figure of flow field and boundaries.

in which **A** and **B** are called the influence matrices, and **u** and **q** are the vectors containing the nodal potential and flux of the boundary elements model, respectively.

If a constant potential is prescribed as the boundary condition, no flux will be generated. Thus, the sum of the terms in each row of **A** must be zero. This allows the diagonal terms of **A**, which include the coefficients c_i's, to be calculated by summing the off-diagonal terms in the same row and reversing the sign.

3.5. Zero-order potential

To calculate the zeroth-order potential associated with steady flow, we define $\phi^{(0)} = v_i\overline{\phi}^{(0)}$. The boundary conditions for $\overline{\phi}^{(0)}$ are

$$\nabla\overline{\phi}^{(0)} \cdot \mathbf{n}^{(0)}|_{\text{wall}} = 0, \quad \nabla\overline{\phi}^{(0)} \cdot \mathbf{n}^{(0)}|_{\text{inflow}} = 1, \tag{37, 38}$$

$$\nabla\overline{\phi}^{(0)} \cdot \mathbf{n}^{(0)}|_{\text{outflow}} = k, \quad \nabla\overline{\phi}^{(0)} \cdot \mathbf{n}^{(0)}|_{\text{rigidwall}} = 0, \tag{39, 40}$$

and thus, $\overline{\phi}^{(0)}$ is only dependent on the shell geometry. The distribution of $\overline{\phi}^{(0)}$ at all of the boundary nodes is determined by applying the boundary conditions given in Eqs. (37)–(40) to Eq. (36).

3.6. First-order potential

The first-order potential is governed by the Laplace equation and satisfies Eq. (36) which can be decomposed into the following form:

$$\mathbf{A}_{11}\mathbf{u}_{\text{o}} + \mathbf{A}_{12}\mathbf{u}_{\text{wr}} - \mathbf{B}_{11}\mathbf{q}_{\text{o}} - \mathbf{B}_{12}\mathbf{q}_{\text{wr}} = \mathbf{0}, \tag{41}$$

$$\mathbf{A}_{21}\mathbf{u}_{\text{o}} + \mathbf{A}_{22}\mathbf{u}_{\text{wr}} - \mathbf{B}_{21}\mathbf{q}_{\text{o}} - \mathbf{B}_{22}\mathbf{q}_{\text{wr}} = \mathbf{0}, \tag{42}$$

where $\mathbf{u}_{\text{o}}$ is a vector of the potential values at the outflow nodes, and $\mathbf{u}_{\text{wr}} = [\mathbf{u}_{\text{w}}^{\text{T}}\ \mathbf{u}_{\text{r}}^{\text{T}}]^{\text{T}}$ is a vector containing the potential values at the wall nodes $\mathbf{u}_{\text{w}}$ and the remaining nodes $\mathbf{u}_{\text{r}}$. Furthermore, the vectors $\mathbf{q}_{\text{o}}$ and $\mathbf{q}_{\text{wr}}$ consist of the nodal fluxes corresponding to $\mathbf{u}_{\text{o}}$ and $\mathbf{u}_{\text{wr}}$, respectively. Eq. (42) can be solved for $\mathbf{u}_{\text{wr}}$ to obtain

$$\mathbf{u}_{\text{wr}} = \mathbf{A}_{22}^{-1}(\mathbf{B}_{21}\mathbf{q}_{\text{o}} + \mathbf{B}_{22}\mathbf{q}_{\text{wr}} - \mathbf{A}_{21}\mathbf{u}_{\text{o}}). \tag{43}$$

Using Eq. (43) in Eq. (41) yields

$$\mathbf{A}^*\mathbf{u}_{\text{o}} - \mathbf{B}^*\mathbf{q}_{\text{o}} = \mathbf{C}\mathbf{q}_{\text{wr}}, \tag{44}$$

where

$$\mathbf{A}^* = \mathbf{A}_{11} - \mathbf{A}_{12}\mathbf{A}_{22}^{-1}\mathbf{A}_{21}, \tag{45}$$

$$\mathbf{B}^* = \mathbf{B}_{11} - \mathbf{A}_{12}\mathbf{A}_{22}^{-1}\mathbf{B}_{21}, \tag{46}$$

$$\mathbf{C} = \mathbf{B}_{12} - \mathbf{A}_{12}\mathbf{A}_{22}^{-1}\mathbf{B}_{22}. \tag{47}$$

By solving Eq. (44) for $\mathbf{q}_{\text{o}}$ and substituting the result into Eq. (43), one can obtain

$$\mathbf{u}_{\text{wr}} = \mathbf{K}\mathbf{u}_{\text{o}} + \mathbf{M}\mathbf{q}_{\text{wr}}, \tag{48}$$

in which the following definitions are used:

$$\mathbf{K} = \mathbf{A}_{22}^{-1}(\mathbf{B}_{21}\mathbf{B}^{*^{-1}}\mathbf{A}^* - \mathbf{A}_{21}), \tag{49}$$

$$\mathbf{M} = \mathbf{A}_{22}^{-1}(\mathbf{B}_{21}\mathbf{B}^{*^{-1}}\mathbf{C}^* + \mathbf{B}_{22}). \tag{50}$$

The boundary-condition equations (21) and (25) give $\mathbf{q}_{\text{r}} = \mathbf{0}$. Therefore, Eq. (44) can be simplified to

$$\mathbf{A}^*\mathbf{u}_{\text{o}} - \mathbf{B}^*\mathbf{q}_{\text{o}} = \mathbf{C}^*\mathbf{q}_{\text{w}}, \tag{51}$$

and the first-order potential on the wall can be evaluated using Eq. (48):

$$\mathbf{u}_{\text{w}} = \mathbf{K}^*\mathbf{u}_{\text{o}} + \mathbf{M}^*\mathbf{q}_{\text{w}}, \tag{52}$$

where $\mathbf{C}^*$, $\mathbf{K}^*$ and $\mathbf{M}^*$ are the sub-matrices of $\mathbf{C}$, $\mathbf{K}$ and $\mathbf{M}$, respectively, that correspond to the wall nodes. Eq. (52) illustrates the velocity potential at the wall nodes, which is to be directly determined in terms of the outflow potential and the flux on the wall. Using the modal expansion series in Eqs. (2) and (3) and inserting Eq. (13) into Eq. (15), one can state

$$\mathbf{q}_{\mathrm{w}} = -v_i \mathbf{E}\boldsymbol{\xi} - \mathbf{F}\dot{\boldsymbol{\xi}}, \tag{53}$$

where

$$\mathbf{E}_{i,j} = (\nabla\overline{\phi}^{(0)} \cdot (\mathbf{n}^{(0)} \times \overline{\boldsymbol{\theta}}_j))|_{\text{node } i}, \tag{54}$$

$$\mathbf{F}_{i,j} = (\overline{\mathbf{e}}_j \cdot \mathbf{n}^{(0)})|_{\text{node } i}. \tag{55}$$

Furthermore, Eq. (24) relates the first-order velocity potential and its normal flux at the outflow boundary as follows:

$$\mathbf{q}_{\mathrm{o}} = -\frac{1}{kv_i}\dot{\mathbf{u}}_{\mathrm{o}}, \tag{56}$$

Introducing Eqs. (53) and (56) into Eq. (51) yields the following governing equation for the first-order potential at the outflow boundary:

$$\frac{1}{kv_i}\mathbf{B}^*\dot{\mathbf{u}}_{\mathrm{o}} + \mathbf{A}^*\mathbf{u}_{\mathrm{o}} = -v_i\mathbf{C}^*\mathbf{E}\boldsymbol{\xi} - \mathbf{C}^*\mathbf{F}\dot{\boldsymbol{\xi}}, \tag{57}$$

3.6.1. Modal analysis of the first-order potential

Assuming a solution of the form $\mathbf{u}_{\mathrm{o}} = \overline{\mathbf{u}}_n \exp(kv_i\lambda_n t)$, the homogenous parts of Eq. (57) can be rewritten as the eigenvalue equation

$$(\mathbf{B}^*\lambda_n + \mathbf{A}^*)\overline{\mathbf{u}}_n = \mathbf{0}, \tag{58}$$

which gives the flow eigenvalues λ_n and the corresponding mode-shapes $\overline{\mathbf{u}}_n$. The flow mode-shapes are indeed the trivial solutions of the first-order potential that satisfy the homogenous problem. The matrices $\mathbf{B}^*$ and $\mathbf{A}^*$ are not symmetric and thus the adjoint eigenvalue problem of Eq. (58) can be written as

$$(\mathbf{B}^{*^{\mathrm{T}}}\lambda_n + \mathbf{A}^{*^{\mathrm{T}}})\overline{\mathbf{v}}_n = \mathbf{0}, \tag{59}$$

where the $\overline{\mathbf{v}}_n$s are the left eigenvectors. The eigenvectors of Eqs. (58) and (59) satisfy the following bi-orthogonality relations:

$$\overline{\mathbf{v}}_n^{\mathrm{T}}\mathbf{B}^*\overline{\mathbf{u}}_m = \begin{cases} 1, & n = m, \\ 0, & n \neq m, \end{cases} \tag{60}$$

$$\overline{\mathbf{v}}_n^{\mathrm{T}}\mathbf{A}^*\overline{\mathbf{u}}_m = \begin{cases} \lambda_n, & n = m, \\ 0, & n \neq m. \end{cases} \tag{61}$$

It is a common procedure in modal analysis techniques to write the solution of the non-homogeneous equation (57) as a sum of the natural mode-shapes; i.e,

$$\mathbf{u}_{\mathrm{o}} = \sum_{m=1}^{N_F} \overline{\mathbf{u}}_m \eta_m(t) = \overline{\mathbf{U}}\boldsymbol{\eta}, \tag{62}$$

in which N_F is the number of flow modes, $\boldsymbol{\eta}$ is the vector of the generalized modal coordinates of the first-order potential and $\overline{\mathbf{U}}$ is a matrix whose columns are the aforementioned eigenvectors. Substituting Eq. (62) into Eq. (57), pre-multiplying by $\overline{\mathbf{v}}_n^{\mathrm{T}}$ and using the bi-orthogonality relations (60) and (61) results in the following governing equations for the modal coordinates of the first-order flow:

$$\frac{1}{kv_i}\dot{\boldsymbol{\eta}} + \boldsymbol{\Lambda}\boldsymbol{\eta} = -v_i\underbrace{\overline{\mathbf{V}}^{\mathrm{T}}\mathbf{C}^*\mathbf{E}}_{\mathbf{E}^*}\boldsymbol{\xi} - \underbrace{\overline{\mathbf{V}}^{\mathrm{T}}\mathbf{C}^*\mathbf{F}}_{\mathbf{F}^*}\dot{\boldsymbol{\xi}}, \tag{63}$$

where $\boldsymbol{\Lambda}$ is a diagonal matrix, defined as $\boldsymbol{\Lambda}_{n,n} = \lambda_n$, and $\overline{\mathbf{V}}$ is a matrix whose columns are the adjoint eigenvectors of $\overline{\mathbf{U}}$.

4. Coupled fluid–structure dynamics

If the gravitational acceleration is neglected, the unsteady Bernoulli equation for the fluid pressure can be written as

$$p = p_i + \tfrac{1}{2}\rho(v_i^2 - |\nabla\phi|^2) - \rho\dot{\phi}, \tag{64}$$

where p_i is the inflow pressure. Substituting Eq. (8) into Eq. (64) results in the following expressions for the zero and first-order pressures on the shell:

$$p^{(0)} = p_i + \tfrac{1}{2}\rho v_i^2(1 - |\nabla\overline{\phi}^{(0)}|^2), \tag{65}$$

$$p^{(1)} = -\rho(\dot{\phi}^{(1)} + v_i\nabla\overline{\phi}^{(0)} \cdot \nabla\phi^{(1)}). \tag{66}$$

If the ambient pressure on the shell is p_a, the virtual work principle allows the generalized structural forces to be calculated by the following integral over the fluid–shell interface:

$$\mathbf{s}_i = \int_{\text{wall}} (\overline{\mathbf{e}}_i \cdot \mathbf{n}^{(0)})(p - p_a)\,\mathrm{d}S \approx \int_{\text{wall}} (\overline{\mathbf{e}}_i \cdot \mathbf{n}^{(0)})p^{(1)}\,\mathrm{d}S + \int_{\text{wall}} (\overline{\mathbf{e}}_i \cdot \mathbf{n}^{(0)})(p^{(0)} - p_a)\,\mathrm{d}S. \tag{67}$$

The generalized structural forces can be evaluated by integrating over the wall boundary elements to obtain

$$\mathbf{s}_i = -\rho\sum \mathbf{R}_{ij}\dot{\mathbf{u}}_j - \rho v_i \sum \mathbf{S}_{ij}\mathbf{u}_j + \mathbf{s}_{0_i}, \tag{68}$$

where

$$\mathbf{R}_{ij} = \int_{S_j} (\overline{\mathbf{e}}_i \cdot \mathbf{n}_j^{(0)})\mathbf{N}_j|\mathbf{J}_j|\,\mathrm{d}x_1\,\mathrm{d}x_2, \tag{69}$$

$$\mathbf{S}_{ij} = \int_{S_j} (\overline{\mathbf{e}}_i \cdot \mathbf{n}_j^{(0)})(\nabla\overline{\phi}^{(0)} \cdot \mathbf{J}_j^{\mathrm{T}-1}[\partial/\partial x_1 \;\; \partial/\partial x_2 \;\; 0]^{\mathrm{T}}\mathbf{N}_j)|\mathbf{J}_j|\,\mathrm{d}x_1\,\mathrm{d}x_2, \tag{70}$$

$$\mathbf{s}_{0i} = \int_{\text{wall}} (\overline{\mathbf{e}}_i \cdot \mathbf{n}_j^{(0)})(p^{(0)} - p_a)\,\mathrm{d}S. \tag{71}$$

Eq. (68) can be written for all of the structural modes to obtain the following equation:

$$\mathbf{s} = -\rho\overline{\mathbf{R}}\dot{\mathbf{u}}_{\mathrm{w}} - \rho v_i\overline{\mathbf{S}}\mathbf{u}_{\mathrm{w}} + \mathbf{s}_0, \tag{72}$$

where $\overline{\mathbf{R}}$ and $\overline{\mathbf{S}}$ are the assembled forms of $\mathbf{R}$ and $\mathbf{S}$, respectively. This equation relates the generalized structural forces to the first-order potential on the wall. Introducing $\mathbf{u}_{\mathrm{w}}$ from Eq. (52) into Eq. (72), and with the help of Eqs. (53) and (62), the vector of generalized structural forces can be expressed in terms of the structural and fluid modal coordinates as follows:

$$\mathbf{s} = -\rho(\mathbf{M}_f\ddot{\boldsymbol{\xi}} + v_i\mathbf{C}_f\dot{\boldsymbol{\xi}} + v_i^2\mathbf{K}_f\boldsymbol{\xi} + \mathbf{C}_f'\dot{\boldsymbol{\eta}} + v_i\mathbf{K}_f'\boldsymbol{\eta}) + \mathbf{s}_0, \tag{73}$$

where

$$\mathbf{M}_f = \overline{\mathbf{R}}\mathbf{M}^*\mathbf{F}, \quad \mathbf{C}_f = \overline{\mathbf{R}}\mathbf{M}^*\mathbf{E} + \overline{\mathbf{S}}\mathbf{M}^*\mathbf{F}, \quad \mathbf{K}_f = \overline{\mathbf{S}}\mathbf{M}^*\mathbf{E}, \tag{74, 75, 76}$$

$$\mathbf{C}_f' = \overline{\mathbf{R}}\mathbf{K}^*\overline{\mathbf{U}}, \quad \mathbf{K}_f' = \mathbf{S}\mathbf{K}^*\overline{\mathbf{U}}. \tag{77, 78}$$

The combination of Eqs. (4), (63) and (73) gives the following governing equations of the coupled fluid–structure dynamics:

$$\begin{bmatrix} \mathbf{0} & \mathbf{I} & \mathbf{0} \\ \mathbf{I} + \rho\mathbf{M}_f & \boldsymbol{\Gamma} + \rho v_i\mathbf{C}_f & \rho\mathbf{C}_f \\ \mathbf{0} & kv_i\mathbf{F}^* & \mathbf{I} \end{bmatrix} \begin{bmatrix} \dot{\boldsymbol{\xi}}^* \\ \dot{\boldsymbol{\xi}} \\ \dot{\boldsymbol{\eta}} \end{bmatrix} + \begin{bmatrix} -\mathbf{I} & \mathbf{0} & \mathbf{0} \\ \mathbf{0} & \boldsymbol{\Omega} + \rho v_i^2\mathbf{K}_f & \rho v_i\mathbf{K}_f \\ \mathbf{0} & kv_i^2\mathbf{E}^* & kv_i\boldsymbol{\Lambda} \end{bmatrix} \begin{bmatrix} \boldsymbol{\xi}^* \\ \boldsymbol{\xi} \\ \boldsymbol{\eta} \end{bmatrix} = \begin{bmatrix} \mathbf{0} \\ \mathbf{s}_0 \\ \mathbf{0} \end{bmatrix}, \tag{79}$$

where $\boldsymbol{\xi}^* = \dot{\boldsymbol{\xi}}$. Eq. (79) describes a reduced-order model that can be employed to determine the linear instability of shells conveying fluid.

Results in the literature show that the non-linearity of the potential flow model does not have a significant effect on the instability margins of the coupled fluid–shell system (Lakis and Laveau, 1991). Accordingly, for the cases in which the potential flow assumption is valid, Eq. (79) may be used for stability analysis of the fluid–shell system. However, due to the limitations of the modal analysis technique, the major limitation of the obtained model arises from the linear structural model.

5. Numerical examples

In this section, two examples are provided to verify the results of the present model in stability analysis of fluid-conveying shells. Then, two examples are considered to examine the application of the model to shells with more complex geometries. In all examples, the model parameters and structural and flow mode numbers are chosen so that the results converge to within a maximum 0.1% error.

5.1. Verification; clamped–clamped pipe and cylindrical shell

Many research projects in FSI problems are dedicated to cylindrical pipes and shells. As the first verification example, the instability of a clamped–clamped cylindrical fluid pipe is considered, and the results are compared with those of Païdoussis (1998). Païdoussis (1998) has carried out detailed investigations on the stability of pipes based on Euler–Bernoulli beam theory for the structural dynamics modeling and slender body theory for the unsteady flow.

Fig. 3 shows a long cylinder with a length-to-radius ratio of $L/r = 40$ and inflow/outflow boundaries at $L_i/r = 5$ and $L_o/r = 20$. The fluid mass ratio is defined as $\beta = m_f/(m + m_f)$ where m and m_f are the mass per unit length of the structure and the fluid. Furthermore, the reference velocity and frequency are defined as $v_0 = \sqrt{EI/m_f L^2}$ and $\omega_0 = \sqrt{EI/(m + m_f)L^4}$, respectively, where EI is the bending rigidity of the pipe section and L is the pipe length. The stability of the pipe is studied via the present model, using the lowest three natural structural modes and 10 flow modes. Figs. 4(a) and (b) show dimensionless values of the frequency ω/ω_0 and damping σ/ω_0 versus the dimensionless flow speed v_i/v_0 for the cases $\beta = 0.1$ and 0.8, respectively. For the case $\beta = 0.1$, Fig. 4(a) shows that the first three bending modes of the pipe diverge at the critical velocities $\overline{v}_i = 6.32$, 9.07, and 12.57. These results are in a very good agreement with those of Païdoussis (1998), which were $\overline{v}_i = 6.28$, 8.99, and 12.56. For the case $\beta = 0.8$, Fig. 4(b) shows that when the flow velocity is increased, a divergence instability occurs at $\overline{v}_i = 6.32$. Then, the pipe becomes stable at $\overline{v}_i = 9.07$, until a flutter instability arises at $\overline{v}_i = 9.6$. Furthermore, Fig. 4(b) shows a divergence instability at $\overline{v}_i = 12.56$. Very good agreement between the present results and those of Païdoussis (1998) can be seen.

The second verification example is a cylindrical shell with simply supported ends, which was considered by Amabili et al. (1999a). The cylinder is made of steel with a Young's modulus of $E = 206\,\text{GPa}$, a density of $\rho = 7850\,\text{kg/m}^3$ and a Poisson's ratio of $\nu = 0.3$ and contains flowing water with a density of $\rho_f = 1000\,\text{kg/m}^3$. The length-to-radius ratio of the cylinder is $L/r = 2$ and the thickness-to-radius ratio is $t/r = 0.01$.

The lowest frequency of the empty shell is associated with the wave number $n = 5$ and the longitudinal half-waves $m = 1$. Amabili et al. (1999a) presented results of a stability analysis on the cylinder, considering two modes with $n = 5$ and $m = 1, 2$ using the models proposed by Païdoussis and Denise (1972) and by Weaver and Unny (1973). The present fluid–structure model is employed with the flow boundary element model for eight flow modes, as shown in Fig. 5, to determine the stability conditions of the shell. Fig. 6 shows a comparison of the obtained results from this stability

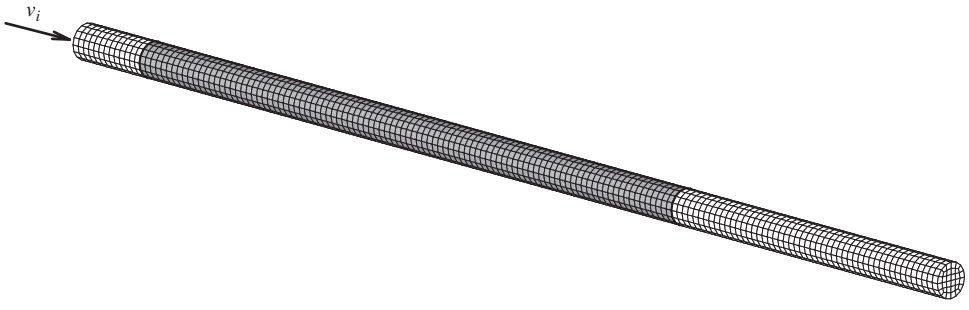

Fig. 3. Boundary element model of the clamped–clamped beam.

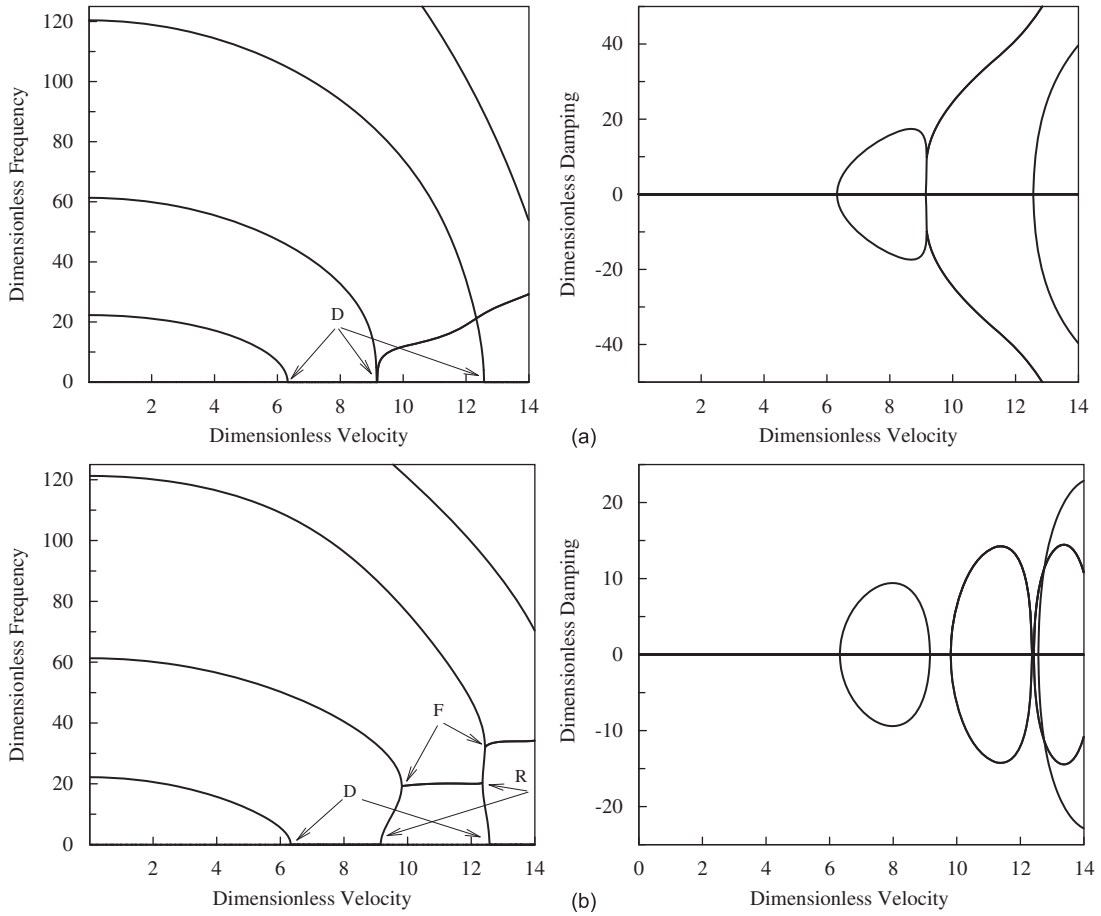

Fig. 4. Plots of dimensionless damping and frequency versus dimensionless flow speed for the clamped-clamped pipe: (a) $\beta = 0.1$; (b) $\beta = 0.8$.

analysis of the cylinder and results given by Amabili et al. (1999a). This figure shows the dimensionless values of the damping σ/ω_0 and frequency $\overline{\omega} = \omega/\omega_0$ versus the dimensionless flow speed $\overline{v} = v_i/v_0$, where $\omega_0 = (\pi^2/L^2)[D/\rho t]^{0.5}$, $v_0 = L\omega_0$ and $D = Et^3/12(1-\nu^2)$. The present results are in very good agreement with those obtained by the model of Weaver and Unny (1973). Fig. 6 shows that the shell experiences a divergence at $\overline{v} = 3.63$. If the flow speed increases, then the cylinder will be re-stabilized at $\overline{v} = 4.73$, and then a coupled-mode flutter occurs at $\overline{v} = 5.12$.

Fig. 7 shows the damping and frequency of the fluid–shell system versus the dimensionless flow speed when the eight lowest structural modes are used. Fig. 7 shows that there is no stable region after the first mode diverges, and the higher structural modes will diverge.

5.2. A cubic shell

The boundary element model of a shell made of four square plates is shown in Fig. 8. The thickness ratio of the plate is $t/L = 0.005$, where L stands for the plate length. The shell is clamped at both ends, and its material properties and the reference values of frequency and flow speed are defined as for the aforementioned cylindrical shell. The fluid–structure model is constructed using the eight lowest structural modes and eight flow modes. Fig. 9 illustrates the four lowest natural mode shapes of the cube along with the corresponding dimensionless natural frequencies. Fig. 10 shows the dimensionless damping and frequency of the structural modes versus the dimensionless flow speed. The results show that the first structural mode diverges at $\overline{v} = 0.42$.

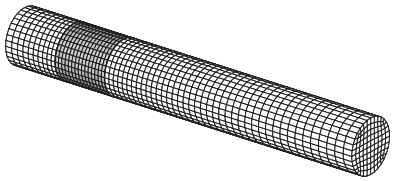

Fig. 5. Boundary element model of the simply supported cylindrical shell.

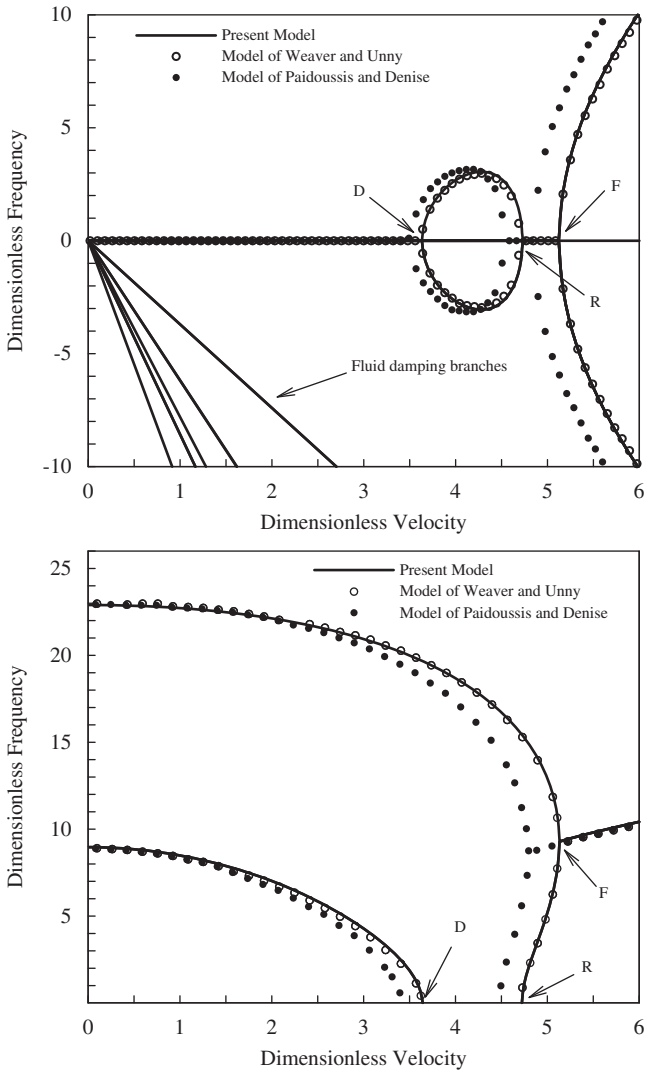

Fig. 6. Comparison of the results obtained for dimensionless damping and frequency of the simply supported cylindrical shell using the results of the model of Païdoussis and Denise and the model of Weaver and Unny [from Amabili et al. (1999a)].

5.3. An elbow shell

The last example is a right-angle elbow shell, as shown in Fig. 11. The viscosity of an actual fluid may cause rotational flow and flow separation in an elbow shell; however, using the proposed model for an approximately inviscid flow provides satisfactory results for the stability margin of the fluid–shell system. The main purpose of presenting this problem is to illustrate that the model developed here is capable of modeling general shell geometries. The elbow has a

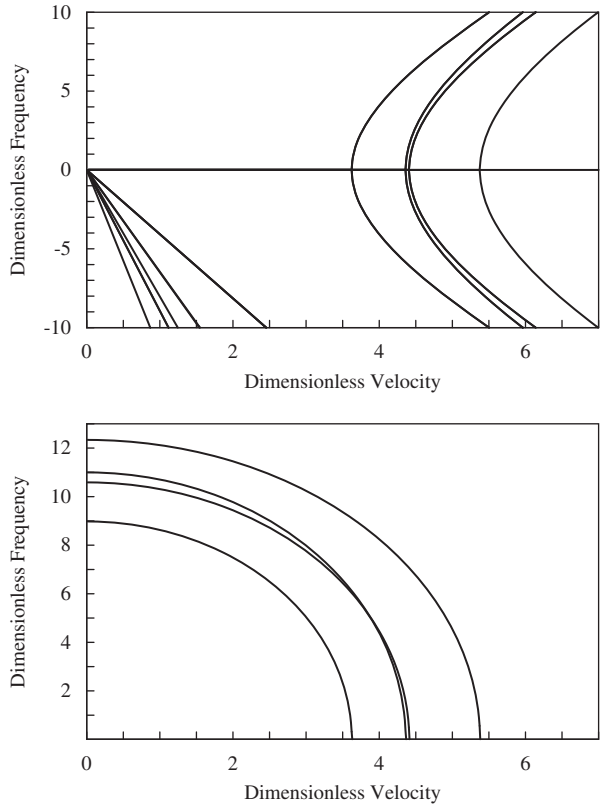

Fig. 7. Dimensionless damping and frequency versus dimensionless flow speed for the simply supported cylindrical shell, considering the eight lowest modes of the cylinder.

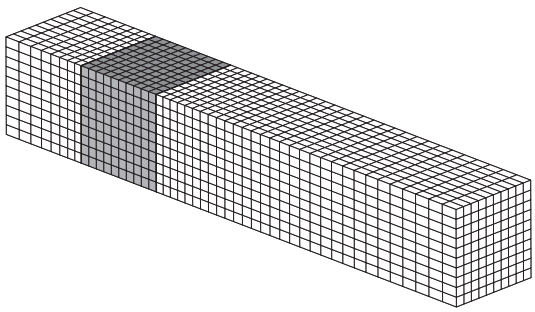

Fig. 8. Boundary elements model of the clamped cubic shell.

circular section and is made of aluminum with a Young's modulus of $E = 70\,\text{GPa}$, a density of $\rho = 2700\,\text{kg/m}^3$ and a Poisson's ratio of $v = 0.3$. The thickness-to-radius ratio of the shell is $t/r = 0.012$, and it is clamped at both ends. The dimensionless parameters are defined as in the cylindrical shell example, and the length considered is $L = 4r + \pi r/2$. The 10 lowest modes of the shell are used for structural modeling, and the four lowest modes are depicted in Fig. 12. The stability margin of the shell is investigated through the plots of dimensionless damping and frequency of the structural modes versus dimensionless flow speed shown in Fig. 13, which shows that the first and second structural modes of the shell diverge at $\overline{v} = 2.86$.

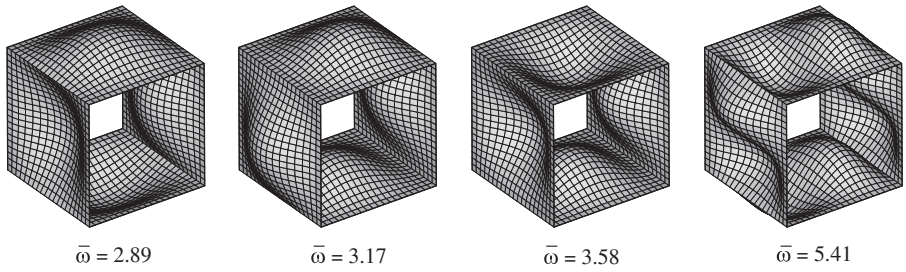

Fig. 9. Four lowest structural modes of the cubic cylinder and corresponding dimensionless frequencies.

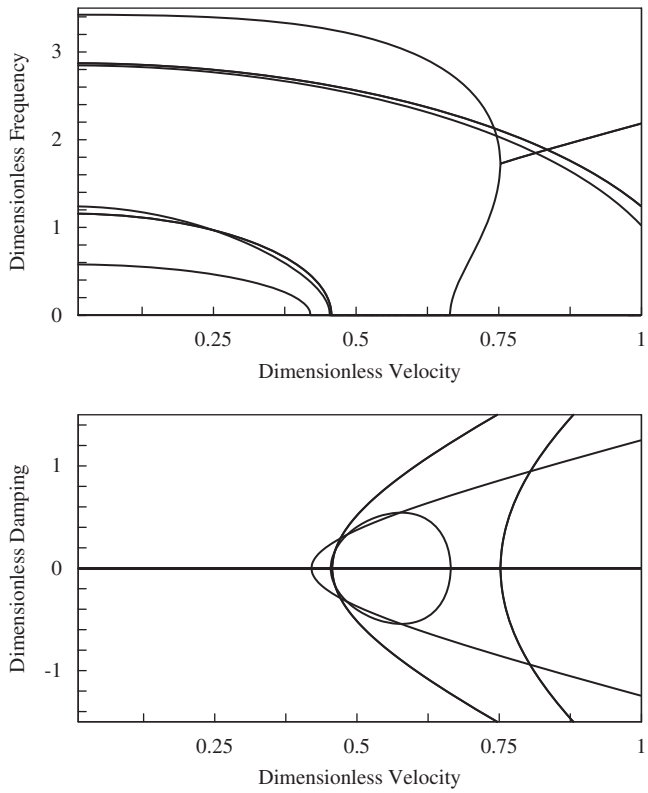

Fig. 10. Dimensionless damping and frequency of the eight lowest modes of the cubic shell versus the dimensionless flow speed.

5.4. The effect of inflow/outflow distances

The inflow/outflow distances L_i and L_o are two major parameters of the present flow model. Properly choosing the minimum values of these parameters avoids the need for a large boundary element model, while the accuracy and convergence of the results are guaranteed. Numerous numerical experiments were performed on the examples above to investigate the convergence of the results as L_i and L_o increase. For instance, the results of the stability analysis of the cylindrical shell with three flow modes with $L_i/r = L_o/r = 0$ (case 1), $L_i/r = 0.5$, $L_o/r = 4$ (case 2) and $L_i/r = 2$, $L_o/r = 10$ (case 3) are given in Fig. 14. The graphs show that the obtained results converge more rapidly as the inflow/outflow distances increase. Fig. 14 shows that the model of case 2 gives results that are very close to the actual values. These case studies were also performed on the other examples, and similar results were achieved. Based on the numerical studies of the effect of increasing L_i and L_o on the instability conditions, we observed that the results converge very quickly as L_i is increased. Furthermore, if L_o is chosen to be two to three times the outlet diameter, the results converge and match the actual values. The case studies show that the effect of the inflow distance on the obtained results is much less than that of the outflow distance and that choosing L_i to be about $0.1L_o$ yields satisfactory results.

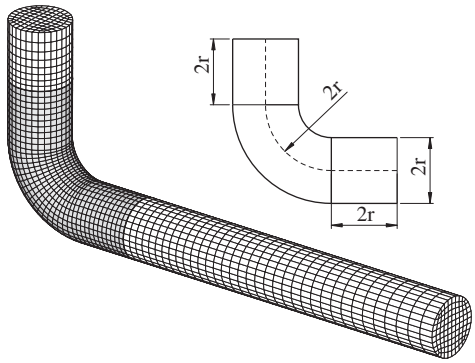

Fig. 11. Boundary element model of the clamped elbow shell.

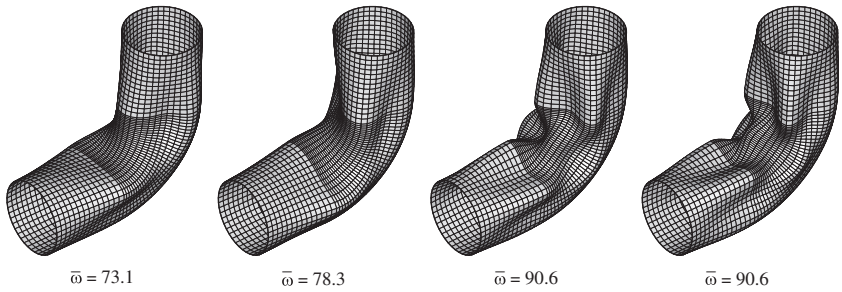

Fig. 12. Four lowest structural modes of the elbow and corresponding dimensionless frequencies.

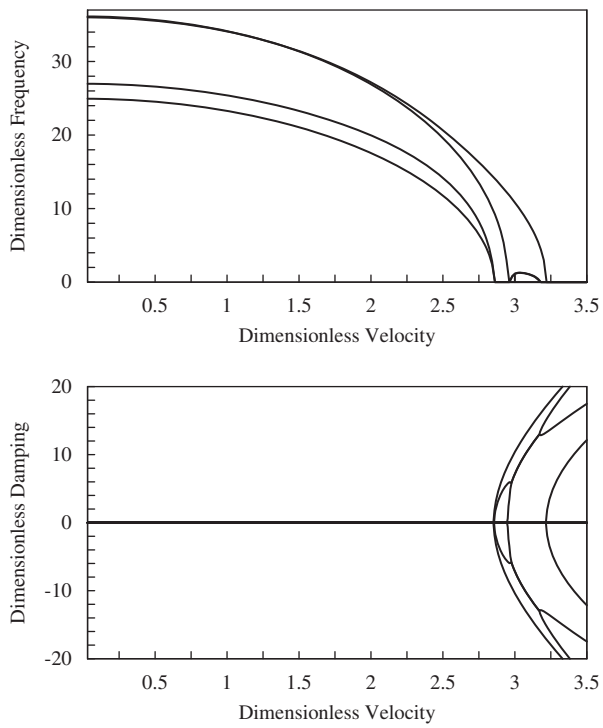

Fig. 13. Dimensionless damping and frequency of the eight lowest modes of the elbow shell versus the dimensionless flow speed.

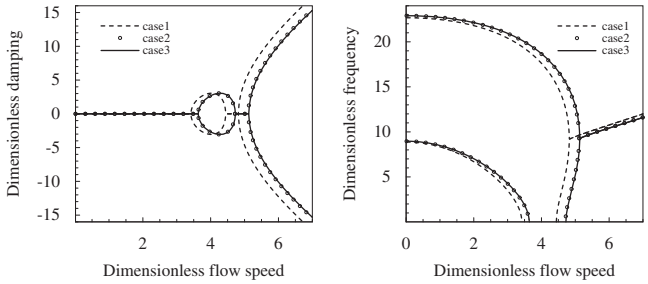

Fig. 14. Variations of dimensionless damping and frequency of the simply supported cylindrical shell versus flow speed for three inflow/outflow distances. Case 1: $L_i/r = L_o/r = 0$; case 2: ($L_i/r = 0.5$, $L_o/r = 4$); case 3: ($L_i/r = 2$, $L_o/r = 10$).

6. Conclusion

A boundary element model was utilized to analyze unsteady potential flow in flexible, fluid-conveying shells. Using an inflow/outflow model, the eigenvalues and mode shapes of the flow in the shell were calculated, and a reduced-order model was developed, which relates the unsteady pressure on the shell to the shell vibrations. The structural dynamics were modeled with modal analysis, and combining this model with the flow field equations yielded the coupled fluid–structure field equations. The results of the developed model were verified against results in the literature. Moreover, the model's capability to perform stability analysis on shells with arbitrary geometries was examined. The major advantage of the present model is the use of the boundary element method along with the modal analysis technique for the fluid and structural dynamics modeling, which provides a reduced-order model for the fluid–structure interaction in the shell. The model is presented with a general formulation, which can easily be used for shells of arbitrary geometry, structural layout, properties and supports.

References

Amabili, M., Pellicano, P., Païdoussis, M.P., 1999a. Nonlinear dynamics and stability of circular cylindrical shells containing flowing fluid. Part I: stability. Journal of Sound and Vibration 225 (4), 655–699.

Amabili, M., Pellicano, P., Païdoussis, M.P., 1999b. Nonlinear dynamics and stability of circular cylindrical shells containing flowing fluid. Part II: large-amplitude vibrations without flow. Journal of Sound and Vibration 228 (5), 1103–1124.

Amabili, M., Pellicano, P., Païdoussis, M.P., 2000a. Nonlinear dynamics and stability of circular cylindrical shells containing flowing fluid. Part III: truncation effect without flow and experiments. Journal of Sound and Vibration 237 (4), 617–640.

Amabili, M., Pellicano, P., Païdoussis, M.P., 2000b. Nonlinear dynamics and stability of circular cylindrical shells containing flowing fluid. Part IV: large-amplitude vibrations with flow. Journal of Sound and Vibration 237 (4), 641–666.

Amabili, M., Garziera, R., 2002a. Vibrations of circular cylindrical shells with nonuniform constraints, elastic bed and added mass. Part II: shells containing or immersed in axial flow. Journal of Fluids and Structures 16 (1), 31–51.

Amabili, M., Garziera, R., 2002b. Vibrations of circular cylindrical shells with nonuniform constraints, elastic bed and added mass. Part III: steady viscous effects on shells conveying fluid. Journal of Fluids and Structures 16 (6), 795–809.

Amabili, M., Pellicano, F., Païdoussis, M.P., 2002. Non-linear dynamics and stability of circular cylindrical shells conveying flowing fluid. Computers and Structures 80 (9–10), 899–906.

Hansson, P.A., Sandberg, G., 2001. Dynamic finite element analysis of fluid-filled pipes. Computer Methods in Applied Mechanics and Engineering 190, 3111–3120.

Karagiozis, K.N., Païdoussis, M.P., Misra, A.K., Grinevich, E., 2005. An experimental study of the nonlinear dynamics of cylindrical shells with clamped ends subjected to axial flow. Journal of Fluids and Structures 20, 801–816.

Karagiozis, K.N., Païdoussis, M.P., Amabili, M., 2007. Effect of geometry on the stability of cylindrical clamped shells subjected to internal fluid flow. Computers and Structures 85, 645–659.

Karagiozis, K.N., Païdoussis, M.P., Amabili, M., Misra, A.K., 2008. Nonlinear stability of cylindrical shells subjected to axial flow: theory and experiments. Journal of Sound and Vibration 309, 637–676.

Kochupillai, J., Ganesan, N., Padmanabhan, C., 2002. A semi-analytical coupled finite element formulation for shells conveying fluids. Computers and Structures 80, 271–286.

Kumar, D.S., Ganesan, N., 2008. Dynamic analysis of conical shells conveying fluid. Journal of Sound and Vibration 310, 38–57.

Lakis, A.A., Laveau, A., 1991. Non-linear dynamic analysis of anisotropic cylindrical shells containing a flowing fluid. International Journal of Solids and Structures 28, 1079–1094.

Modarres-Sadeghi, Y., Païdoussis, M.P., 2009. Nonlinear dynamics of extensible fluid-conveying pipes, supported at both ends. Journal of Fluids and Structures 25, 535–543.

Nguyen, V.B., Païdoussis, M.P., Misra, A.K., 1993. A new outflow model for cylindrical shells conveying fluid. Journal of Fluids and Structures 7 (4), 417–419.
Païdoussis, M.P., Denise, J.P., 1972. Flutter of thin cylindrical shells conveying fluid. Journal of Sound and Vibration 20, 9–26.
Païdoussis, M.P., Li, G.X., 1993. Pipes conveying fluid: a model dynamical problem. Journal of Fluids and Structures 7, 137–204.
Païdoussis, M.P., 1998. Fluid–Structure Interaction: Slender Structures and Axial Flow, vol. 1. Academic Press, London.
Païdoussis, M.P., 2003. Fluid Structure Interaction: Slender Structures and Axial Flow, vol. 2. Elsevier Academic Press, London.
Païdoussis, M.P., 2005. Some unresolved issues in fluid–structure interactions. Journal of Fluids and Structures 20, 874–890.
Selmane, A., Lakis, A.A., 1997. Non-linear dynamic analysis of orthotropic open cylindrical shells subjected to a flowing fluid. Journal of Sound and Vibration 202, 67–93.
Shekari, M.R., Khaji, N., Ahmadi, M.T., 2009. A coupled BE-FE study for evaluation of seismically isolated cylindrical liquid storage tanks considering fluid–structure interaction. Journal of Fluids and Structures 25, 567–585.
Weaver, D.S., Unny, T.E., 1973. On the dynamic stability of fluid-conveying pipes. Journal of Applied Mechanics 40, 48–52.
Zhang, Y.L., Gorman, D.G., Reese, J.M., 2001. A finite element method for modeling the vibration of initially tensioned thin-walled orthotropic cylindrical tubes conveying fluid. Journal of Sound and Vibration 245, 93–112.